Journal of Intelligent and Robotic Systems **36:** 191–208, 2003.

Robotic Welding Systems with Vision-Sensing and Self-learning Neuron Control of Arc Welding Dynamic Process

S. B. CHEN[1], Y. ZHANG[2], T. QIU[1] and T. LIN[1]
[1]*Institute of Welding Engineering, Shanghai Jiaotong University, Shanghai 200030, China; e-mail: rwlab@mail.sjtu.edu.cn*
[2]*Department of Mechanical Engineering, Tsinghua University, Beijing 100084, China*

(Received: 12 February 2002; in final form: 28 June 2002)

Abstract. This paper addresses the vision sensing and neuron control techniques for real-time sensing and control of weld pool dynamics during robotic arc welding. Current teaching playback welding robots are not provided with this real-time function for sensing and control of the welding process. In our research, using composite filtering technology, a computer vision sensing system was established and clear weld pool images were captured during robotic-pulsed Gas Tungsten Arc Welding (GTAW). A corresponding image processing algorithm has been developed to pick up characteristic parameters of the weld pool in real-time. Furthermore, an ANN model of the weld pool dynamic process of robotic-pulsed GTAW was developed. Based on neuron self-learning PSD controller design, the real-time control of weld pool dynamics during the pulsed GTAW process has been realized in robotic systems.

Key words: robotic welding, vision sensing, neuron control, weld pool dynamics.

1. Introduction

Although artificially intelligent methods have been extensively used in the fields of advanced manufacturing and robotic systems for many years [4, 15], teaching playback welding robots have been widely used in welding production. In recent years, much research has been carried out on robotic arc welding, but current teaching play-back robotic welding is open-looped manufacturing process with constant welding parameters, a limited intelligent technique used in welding robotic systems, such that satisfactory weld quality can often not be achieved when welding conditions are greatly changed either due to man-made or other circumstances. As is well known, high-quality welding requires real-time control of weld pool dynamics. Effective detection and control of weld pool dynamic features are puzzling problems for the welding robot and are also key technologies for intelligent welding robots in the future.

Weld penetration is a crucial welding quality parameter. Control of weld penetration is at all times a puzzling problem in automatic or robotic welding [14, 18].

Backside weld width and penetration are direct factors for determining the weld quality. Although the backside bead width could be directly detected from the rear of the work-piece, sensing from the backside is inaccessible in most cases. Therefore, control of weld quality by sensing the topside has become a highly challenging problem in robot welding. A lot of research aims at sensing, modeling and control of the welding dynamic process to improve the weld quality of robotic welding under complex welding conditions [1, 3, 5–7, 9–12, 16].

Recently, it has been attempted to use visual sensing technology in some welding processes, owing to the fact that the visual sensor is not touched or interfered with during the welding process and visual images of the weld pool contain more abundant information about welding dynamics. Kovacevic et al. [5, 6] investigated sensing and control of the weld pool based on visual sensing in GTAW by a high-shutter-speed camera assisted with a pulsed laser for capturing poor weld images. Pietrzak and Packer [9] and Przakovic and Khani [10] developed a coaxial arc weld pool viewing system, which could obtain clear weld pool images by preventing the bright arc core from overpowering the exposure on the CCD target. Suga et al. [11, 12] investigated vision-based sensing and control of the GTAW pool. Some studies on welding path planning and seam tracking by vision sensing were reported in [8, 13, 17].

In our previous research, a double-sided visual sensing system was established [1] for monitoring weld pool dynamics. Through a composite filter system, which included both narrow band filter and neutral density filter, clear weld pool images of pulsed GTAW were captured. The backside weld pool sizes could then be predicted by a backside neural network model. The intelligent control of backside weld width was realized [1, 3].

Modeling and control of the welding process has been a perplexing difficulty for many years because the arc welding process is inherently variable, nonlinear, time varying and strongly coupling. Conventional models and control methods cannot precisely describe and control the arc welding process. Lim et al. [7] proposed an artificial neural network model to predict weld penetration depth, topside and backside width on-line from the detected surface temperature during the GMAW process. Tzafestas and Kyriannakis [16] presented a hierarchical MIMO predictive control scheme for the regulation of GMA welding thermal characteristics. Using fuzzy logic control and artificial network methodologies, we presented a self-learning fuzzy neural control scheme for generally uncertain processes, which dealt with the problem of uncertain systems with time delays in the arc welding process [2]. In Suga et al. [11], an adaptive control system using an artificial neural network was proposed for TIG welding control. The ANN model inputs were the weld pools' characteristic parameters and welding parameters, and the output was the change in welding current.

It must be emphasized that the sensing and control of the weld penetration above mainly focused on the traditional automatic welding process, and welding

conditions, such as a certain welding direction and position of the arc torch. Few studies are aimed at multi-joint welding robots for the sensing and control of weld penetration. Weld quality control in multi-joint robot systems is vastly different to traditional automatic welding due to the effects of vibration and positional errors on robot movement, which brings some difficulties for real-time welding processing control.

In this research, based on a platform of an arc welding robot with 9 degrees of freedom and a visual sensing system, welding pool characteristics were picked up and analyzed by image processing for real-time control of the welding dynamics, which associates with weld penetration and quality. The welding parameters in the robot systems were regulated to ensure a good weld quality under some uncertain welding conditions during robotic welding.

2. The Robotic Welding Experimental Systems

2.1. THE FUNCTIONAL STRUCTURE OF ROBOTIC WELDING SYSTEMS

The robotic welding systems for real-time control of weld pool dynamics during pulsed GTAW were established as in Figure 1, which included a 6-freedom arc weld manipulator, a 3-freedom work-piece positioner, a computer for weld pool sensing and control (SPPC), welding power source (WP), image processing (IP), visual sensor, etc., the central control computer (CCPC) for the supervision of all the robotic welding systems, the movement control computer for coordinating motion between the manipulator and the positioner. The whole system could be referred to as a flexible weld-manufacturing cell (FWMC). The SPPC was the core of the subsystem for weld pool sensing and control, and realized three functions:

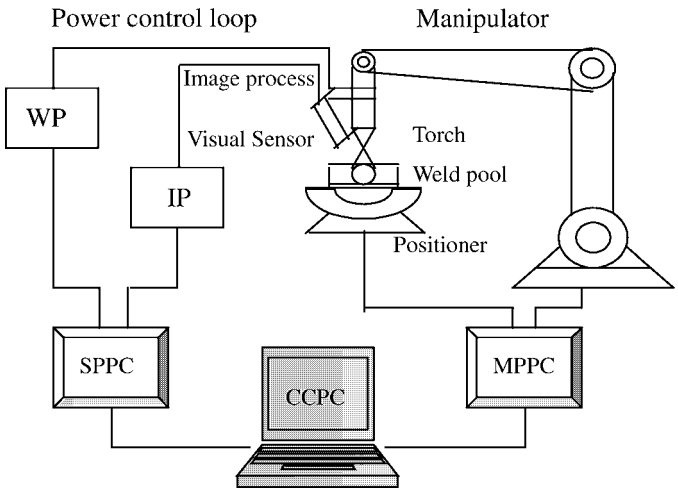

Figure 1. Structure diagram of weld pool sensing and control system during robotic-pulsed GTAW.

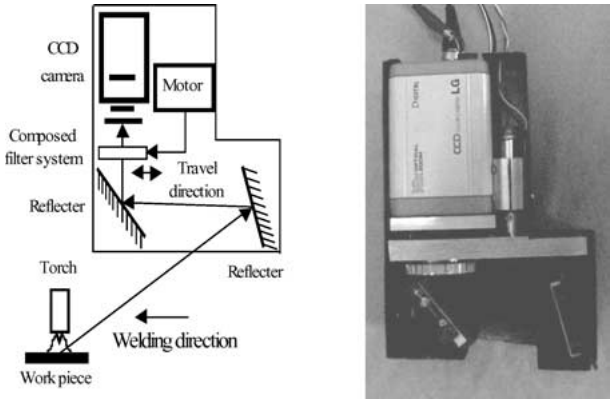

Figure 2. Structure diagram and photograph of robot's image sensor.

communication with the central computer through serial ports, control of the welding power with D/A inverter card and interface card, and control of visual sensor through an image-capturing card. Image signals were transmitted to the SPPC and processed. The SPPC set the welding current through the D/A card, taking image time and the image field size. Those functions were realized through the same controlling computer, which ensured synchronization between image capturing and welding-current setting during robotic arc welding.

2.2. VISION SENSING SUBSYSTEM

The structure diagram and a photograph of the visual sensor are shown in Figure 2. The main element in the visual sensor is a charge-coupled device (CCD) camera. In order to decrease disturbances during robot movement, a two-step reflecting light path system was adopted. Through a composite filter system, which consisted of a neutral density filter and a narrow band filter, weld pool images and arc light entered the CCD camera. The center band of the narrow band filter was 661 nm, half-width was 10 nm, and the peak attenuation ratio of the lens was 83.9%. The sensor was fixed to the rear of the robotic welding torch for as clear a view of the weld pool region as possible. The camera lens center, reflector center and the axis of the torch were set in the same plane.

3. Weld Pool Image Processing

3.1. WELD POOL IMAGES DURING ROBOTIC-PULSED GTAW

In order to obtain satisfactory weld pool images during robotic-pulsed GTAW, visual sensor parameters must be perfectly matched, such as the parameters of the narrow band filter and neutral density filter, CCD camera parameters, current and time of capturing images, etc.

Because of strong arc light during a pulse peak current, the beginning of the pulsed base current time was selected to capture weld pool images. Experimental results showed that good weld pool images could be obtained when the current was 40A. The images from different times corresponding to the pulsed current time sequence in Figure 3 are shown in Figure 4.

A typical pool image of robotic-pulsed GTAW is shown in Figure 5, where nozzle of torch, arc, weld pool and solidified metal can be easily distinguished.

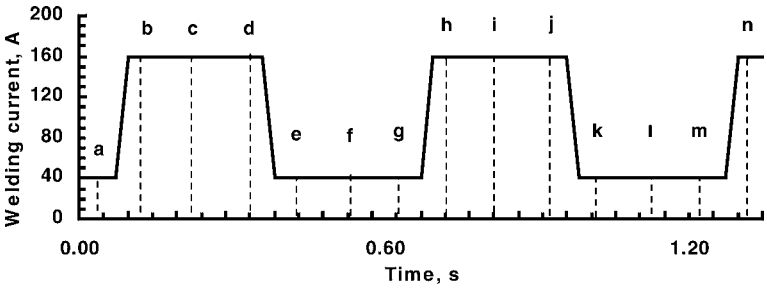

Figure 3. Pulsed current time sequence.

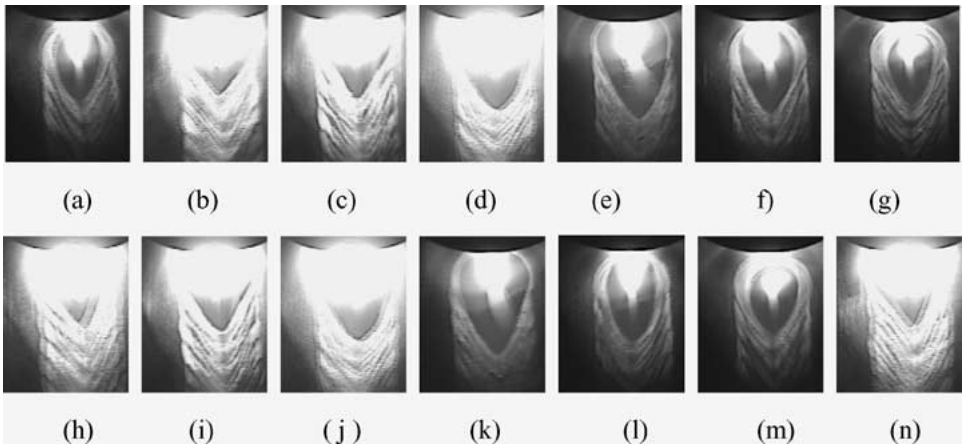

Figure 4. Images from different times.

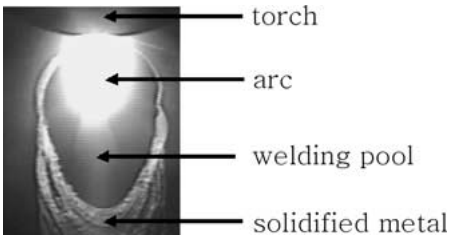

Figure 5. Typical pool image of robotic-pulsed GTAW.

3.2. WELD POOL IMAGE PROCESSING

In order to investigate weld penetration and weld quality, two characteristic parameters of the weld pool, topside maximum width W_{fmax} and topside half-length L_{fmax} as shown in Figure 6 were defined as follows.

Using image processing algorithms designed in this study, the characteristic parameters of weld pools were determined. Usually, a robotic controller cannot ensure that the angle between the direction of sensing and the welding direction is always in accordance with the complicated seams. On the other hand, the torch angle varied during robot welding, which introduced difficulties of image processing. In Figure 7, three typical weld pool images were captured during the welding of an S-shaped seam. Therefore, the algorithm for weld pool image processing must be applicable to the changing of observation direction during robotic arc welding.

The processing of a typical weld pool image is shown in Figure 8. Through a Gauss filter with 7×7 window, the original weld pool image in Figure 5 was smoothed (Figure 8(a)), which decreased the interference noises from the arc light or the signal-transmitting path. The gray distribution property in Figure 9 showed that gray level jumps existed at the weld pool edge points, when the image was scanned from the center point to the exterior. This gray level jump was used to detect the weld pool edge. The center point of the weld pool was right through the arc center, marked as C (shown in Figure 8(b)). The tail point of the weld pool was scanned and marked as point T (Figure 8(b)). The weld pool image was scanned in a direction vertical to CT in the workpiece coordinate system, and scanning ended when a gray level jump was encountered. This point was viewed as the edge point

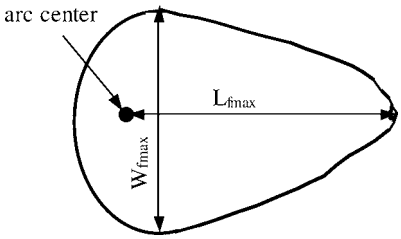

Figure 6. Definition of characteristic parameters of weld pool during robotic-pulsed GTAW.

(a) Image from the right (b) Image from the backside (c) Image from the left

Figure 7. Typical weld pool images during the welding of an S-shaped seam.

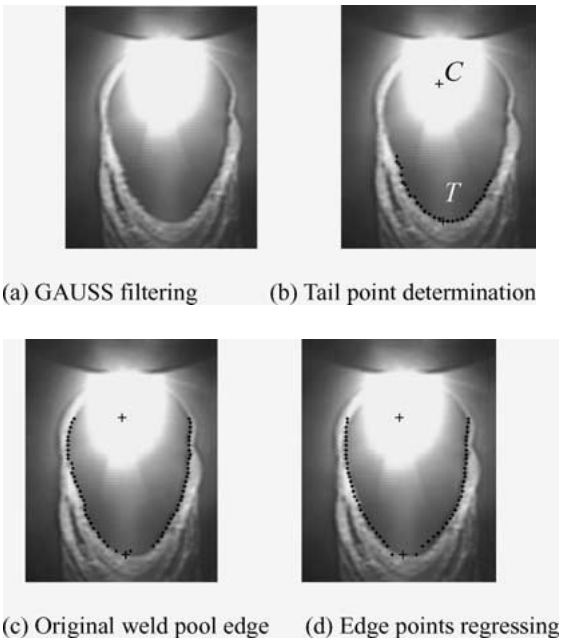

Figure 8. Weld pool image processing for robotic-pulsed GTAW.

of the weld pool shown in Figure 8(c). The results of regressing the edge points is shown in Figure 8(d).

Some experiments below were proposed to veritify the adaptablity of the image-processing algorithms when the observation direction was changed. A weld pool model, whose shape and size were similar to the real weld pools, was positioned such that the torch's axis was vertical to the plane of the weld pool model. By rotating the last robotic joint, the visual sensor observed the weld pool model from various orientations, as shown in Figure 10. The model's characteristic parameters were measured in various observing directions by the arithmetic mentioned above. The actual maximum width of the weld pool model was 6.2 mm, and the half-length was 8.5 mm (shown in Figure 9(a)). Measuring results are shown in Figure 11. We found that the maximum error of the maximum width of the model was 0.15 mm, the average error being 0.06 mm, and the maximum error of the half-length was 0.12 mm, the average error being 0.04 mm. Sensing results showed that the image-processing arithmetic was able to match for the changing of sensing orientation during robotic welding.

3.3. INVESTIGATION OF TORCH HEIGHT AND PITCH ANGLE INFLUENCES ON WELD POOL CHARACTERISTICS

During robotic welding with a vision-sensing system, not only the observing angle of the visual sensor could be changed along with weld torch circumrotation, but

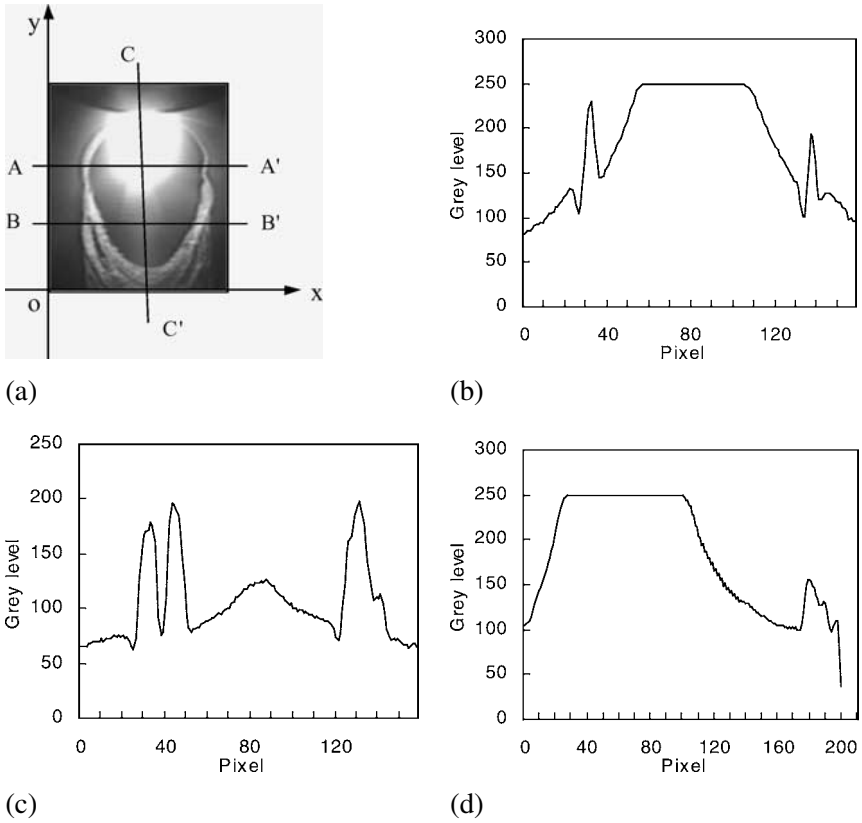

Figure 9. The gray distributions of the weld pool image in different directions: (a) the original image; (b) the direction AA′; (c) the direction BB′; (d) the direction CC′.

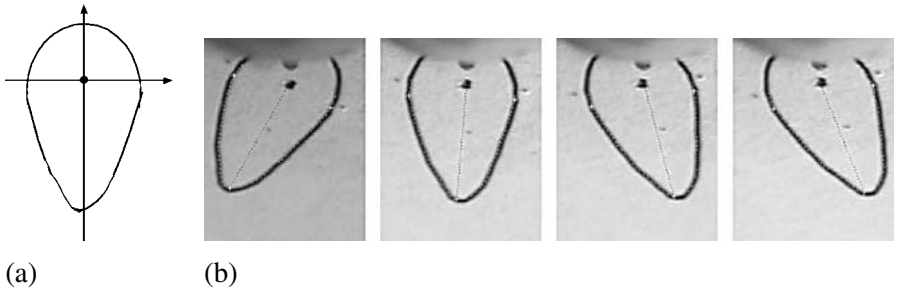

Figure 10. Images of weld pool model observed from various directions: (a) actual shape and size of weld pool model; (b) images of weld pool model from various directions.

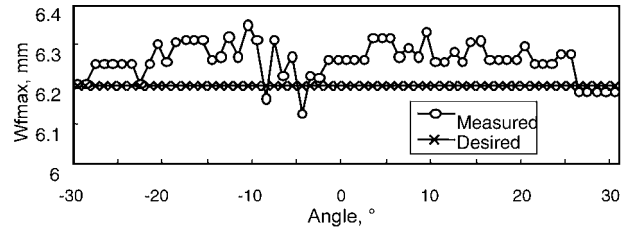

(a) Maximum top width of weld pool

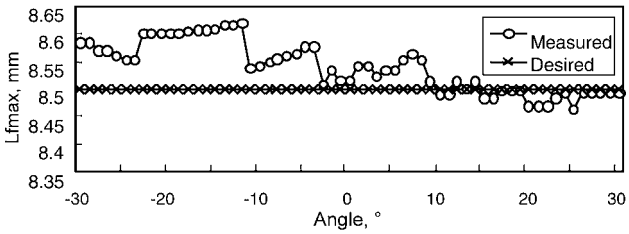

(b) Maximum top half-length of weld pool

Figure 11. Character parameters of weld pool with different observing angles.

also the torch height (arc length) and pitch angle would have some inevitable changes, thus the image quality of the weld pool was obviously influenced. It is necessary to determine an effective and robust range for the welding robot systems under disturbances to torch height (arc length) and pitch angle.

In this welding robot system, the torch height was held by arc sensing and regulation, and the welding experiments were conducted under the following set limits: (1) The inclined angle range between the torch and normal line of the work-piece plane was [−10°–10°]; (2) The arc length could be effectively regulated [1.5–2.5 mm]. The following experiment was completed for analysis of the influences of torch inclined angle and arc length changes on weld pool image characteristics as shown in Figure 11.

Based on weld pool model Figure 9(a), observing from just rear of the weld pool, the center line of the torch was upright to the weld pool plane and through the arc center, the arc length was changed [1.5–2.5 mm] by step-lengths of 0.25 mm. Five images of the weld pool were obtained.

Using corresponding image processing and character picking-up algorithms, the curve of characteristic changes with arc length is shown in Figure 12. The experimental results indicate that, in a limited range of arc length changes, the maximum width error of the topside weld pool was 0.03 mm, and the maximum width error of the topside weld pool was 0.70 mm; and the measured half-length of the weld pool was evidently increased with the increase of arc length.

Figure 13 shows the characteristic changes of the weld pool during welding torch pitch angle changes. Where the pitch angle changed in [−10°–10°], the step-

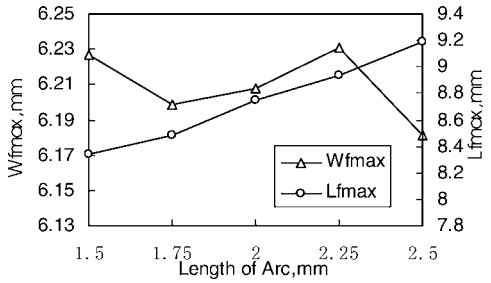

Figure 12. Arc length change influences on picking-up characteristics of weld pool.

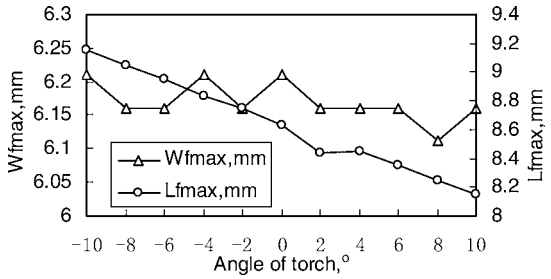

Figure 13. Torch pitch angle changes influence on the character parameters of weld pool.

length was set as 2°. When the pitch angle changed, the maximum width of the topside weld pool had a little fluctuation, the maximum error of weld pool width was 0.1 mm. The pitch angle changes evidently influenced the maximum half-length of the topside weld pool, the maximum error was 0.65 mm, and measured value of the maximum half-length of the topside weld pool decreased as the pitch angle increased.

4. Modeling of the Dynamic Welding Process

Modeling of the welding process is the basis of controller design. An effective model must reflect the actual welding process accurately. Because of the complexity of the weld pool dynamics, conventional modeling methods are not usually suitable for the welding process. Considering the merits of modeling for control systems, in this study, the back-propagation (BP) type of artifical neural net (ANN) was selected to model weld pool dynamic process. Modeling data were obtained from robotic welding experiments. Under the welding conditions shown in Table I and designed pseudorandom sequence inputs, say, Figure 17(a), dynamic sample data of weld pool characteristic parameters were acquired for training the ANN model using real-time visual sensing and image processing during robotic welding.

Table I. Experimental conditions of robotic-pulsed GTAW for obtaining model data

Peak current (A)	Varying from 140 to 180 at random
Pulse duty ratio (%)	Varying from 35 to 70 at random
Pulse frequency (Hz)	1
Traveling speed (mm/s)	3.0
Arc length (mm)	2.0
Flux of argon (l/min)	8.0
Base current (A)	40
Work-piece dimension / mm×mm×mm	250×50×2

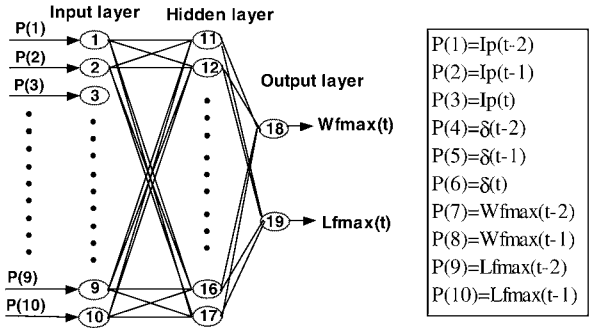

Figure 14. Structure diagram of topside parameters model.

4.1. MODELING OF DYNAMIC CHARACTERISTICS OF THE TOPSIDE WELD POOL

The structure of the topside weld pool dynamic model for robotic pulsed GTAW processes is shown in Figure 14. In this model, welding parameters, which include peak current value I_p and pulse duty ratio δ, were determined as input parameters. Because of heat inertia in the welding process, historical values of welding parameters were also selected as inputs of the dynamic ANN model of the weld pool. For example, $I_p(t-1)$ meant the peak current value of last pulse, and $I_p(t-2)$ meant the peak current value of the last-before-one pulse. Character parameters of weld pool, maximum width (W_{fmax}) and half-length (L_{fmax}), were determined as outputs of the ANN model. Considering the influence of the process continuity, The historical value of weld pool characteristics were also input into the model, e.g., $W_{fmax}(t-1)$, $W_{fmax}(t-2)$ and so on. There are ten inputs and two outputs in the model. The hidden layer in the model contains seven elements, which was determined by the convergence rate of the net model training. The sigmoid function was selected as the nonlinear transfer function of the neurons in the net. The

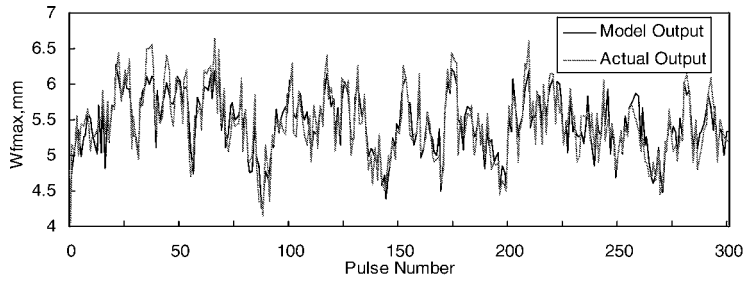

(a) Maximum width of weld pool

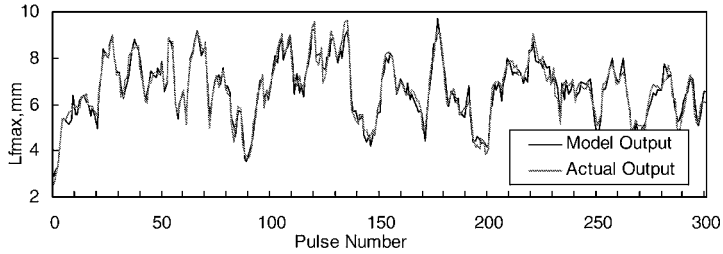

(b) Maximum half-length of weld pool

Figure 15. Comparison of dynamic responses of the weld pool topside model and the actual process.

training results of this model are as follows: maximum absolute error of maximum width of weld pools was 0.50 mm, average error of maximum width was 0.01 mm, and root-mean-square error (RMS) of maximum width was 0.23 mm. The errors of the half-lengths of the weld pools were 0.82 mm, −0.02 mm and 0.34 mm, respectively. The results are shown in Figure 15, one can see that the identified model could approximate a real dynamic welding process.

4.2. MODELING OF DYNAMIC CHARACTERISTICS OF THE BACKSIDE WELD POOL

Generally, topside weld pool width cannot always reflect weld quality accurately, but width change of the backside weld pool is a main characteristic in determining the weld quality. In many cases, the backside weld bead width cannot be sensed and measured in real time. Therefore, a dynamic model of the backside weld pool during robotic pulsed GTAW was established in our study. In order to compare the modeling approximation, two model structures, size neural network model (SNNM) and size and shape neural network model (SSNNM), were designed and are shown in Figure 16. One can see that the SSNNM model is more complicated than the SNNM model. In the figures, definitions of symbols in the model are the same as those in Figure 14. In addition, W_{bmax} means the maximum backside

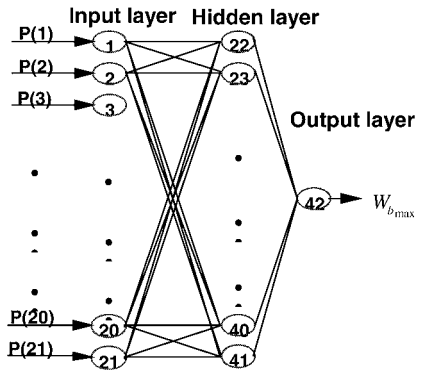

P(1)=I_p(t-2)	P(12)=U_p(t)
P(2)=I_p(t-1)	P(13)=S_{fmid}(t-2)
P(3)=I_p(t)	P(14)=S_{fmid}(t-1)
P(4)=δ(t-2)	P(15)=S_{fmid}(t)
P(5)=δ(t-1)	P(16)=L_{fmax}(t-2)
P(6)=δ(t)	P(17)=L_{fmax}(t-1)
P(7)=V_w(t-2)	P(18)=L_{fmax}(t)
P(8)=V_w(t-1)	P(19)=W_{fmax}(t-2)
P(9)=V_w(t)	P(20)=W_{fmax}(t-1)
P(10)=U_p(t-2)	P(21)=W_{fmax}(t)
P(11)=U_p(t-1)	

(a) The structure of a SNNM neural network model

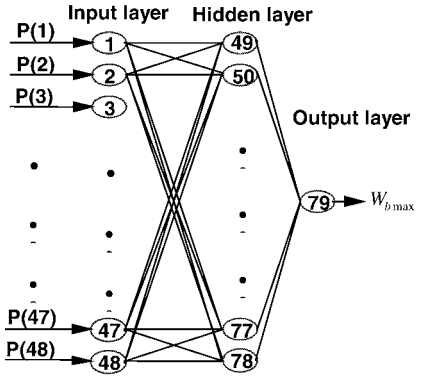

P(1)=I_p(t-2)	P(17)=L_{fmax}(t-1)	P(33)=W_{f5}(t)
P(2)=I_p(t-1)	P(18)=L_{fmax}(t)	P(34)=W_{f6}(t-2)
P(3)=I_p(t)	P(19)=W_{f1}(t-2)	P(35)=W_{f6}(t-1)
P(4)=δ(t-2)	P(20)=W_{f1}(t-1)	P(36)=W_{f6}(t)
P(5)=δ(t-1)	P(21)=W_{f1}(t)	P(37)=W_{f7}(t-2)
P(6)=δ(t)	P(22)=W_{f2}(t-2)	P(38)=W_{f7}(t-1)
P(7)=V_w(t-2)	P(23)=W_{f2}(t-1)	P(39)=W_{f7}(t)
P(8)=V_w(t-1)	P(24)=W_{f2}(t)	P(40)=W_{f8}(t-2)
P(9)=V_w(t)	P(25)=W_{f3}(t-2)	P(41)=W_{f8}(t-1)
P(10)=U_p(t-2)	P(26)=W_{f3}(t-1)	P(42)=W_{f8}(t)
P(11)=U_p(t-1)	P(27)=W_{f3}(t)	P(43)=W_{f9}(t-2)
P(12)=U_p(t)	P(28)=W_{f4}(t-2)	P(44)=W_{f9}(t-1)
P(13)=S_{fmid}(t-2)	P(29)=W_{f4}(t-1)	P(45)=W_{f9}(t)
P(14)=S_{fmid}(t-1)	P(30)=W_{f4}(t)	P(46)=W_{f10}(t-2)
P(15)=S_{fmid}(t)	P(31)=W_{f5}(t-2)	P(47)=W_{f10}(t-1)
P(16)=L_{fmax}(t-2)	P(32)=W_{f5}(t-1)	P(48)=W_{f10}(t)

(b) The structure of SSNNM neural network model

Figure 16. Structure diagram of the backside parameters model.

width of the weld. This ANN model was trained in the same way as the topside parameters model, and the model results were as follows: maximum absolute error was 0.70 mm, average error was 0.03 mm and RMS error was 0.21 mm. Comparing Figure 17(b) with Figure 17(c), one can see that the approximation precision of SSNNM for weld pool dynamics is better than that of the SNNM.

5. Neural Self-learning Control of Weld Pool Dynamics during the Robotic Welding Process

In this study, a neuron self-learning Proportional-Summational-Differential (PSD) controller was designed for the robotic welding process. The main merits of the PSD controller are its modeling of the complicated process and its adaptability. Measuring errors between the actual outputs and the expected outputs, the PSD can

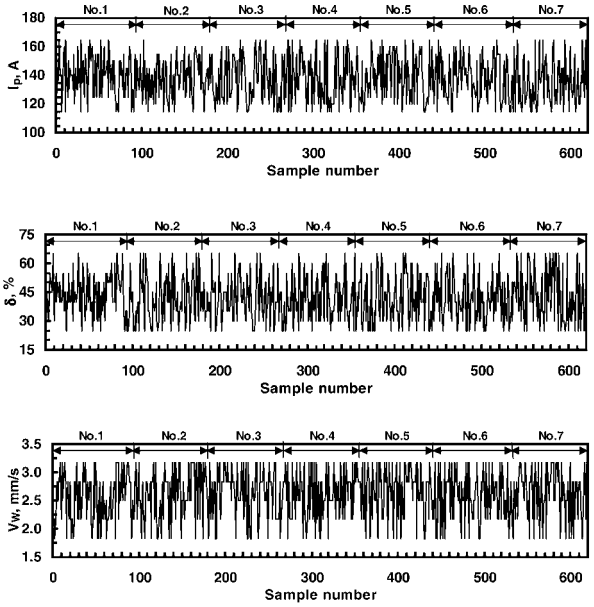

(a) Pseudorandom sequence input singnals

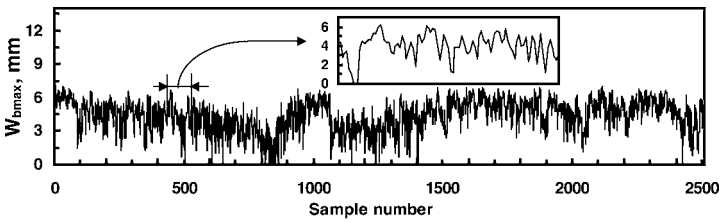

(b) The measured value of maximum backside pool width

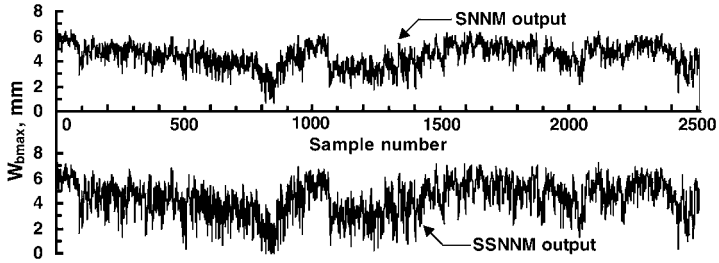

(c) The model output of maximum backside pool width

Figure 17. Comparing the dynamic responses of the backside weld pool model and the actual process.

realize an adaptive control of the process. A neuron self-learning PSD controller's output follows as

$$\Delta u(t) = \omega_1(t)x_1(t) + \omega_2(t)x_2(t) + \omega_3(t)x_3(t) \tag{1}$$

where $u(t)$ is the controlling input, $x_i(t)$ $(i = 1, 2, 3)$ are the input signals of the neuron, and $\omega_i(t)$ $(i = 1, 2, 3)$ is the weight coefficient of $x_i(t)$. $x_i(t)$ is defined as follows: $x_1(t) = e(t)$, $x_2(t) = \Delta e(t)$ and $x_3(t) = \Delta e^2(t)$. $\omega_i(t)$ is regulated continually during neuron learning. The learning rule is

$$\omega_i(t+1) = (1-m)\omega_i(t) + dr_i(t) \tag{2}$$

where $m, d > 0$, d is the learning ratio and

$$r_i(t) = z(t)u(t)\big[e(t) + \Delta e(t)\big] \tag{3}$$

where $z(t)$ is the teaching signal.

To ensure the convergence and robustness of the PSD, the following learning algorithm was adopted:

$$\Delta u(t) = K \sum_{i=0}^{3} \omega'(t)x_i(t) \tag{4}$$

where

$$\omega_i'(t) = \sum_{i=1}^{3} \big|\omega_i(t)\big| \tag{5}$$

and

$$\begin{cases} \omega_1(t+1) = \omega_1(t) + d_I z(t)u(t)\big[e(t) + \Delta e(t)\big], \\ \omega_2(t+1) = \omega_2(t) + d_P z(t)u(t)\big[e(t) + \Delta e(t)\big], \\ \omega_3(t+1) = \omega_3(t) + d_D z(t)u(t)\big[e(t) + \Delta e(t)\big]; \end{cases} \tag{6}$$

here d_P, d_I and d_D are regulated according to the actual system.

Experimental results of robotic welding systems showed that control of the topside characters of the weld pool during the GTAW process could not always ensure an ideal weld penetration or backside weld bead because of different gaps existing between the two work-pieces. Therefore, it was necessary to control the backside dynamic characteristics of the weld pool. In many cases, it is impossible to detect directly the backside dynamic changes of the weld pool. Using the above neural model and neuron self-learning PSD controller, a butt-welding experiment during the pulsed GTAW process was conducted on the welding robot systems. The control system structure is shown in Figure 18. The output value of the PSD controller was the increment of peak current of the pulsed GTAW. During welding, topside parameters of the weld pool were sensed and measured in real-time. The backside weld width W_{mbmax} could be predicted by the topside pool characteristics

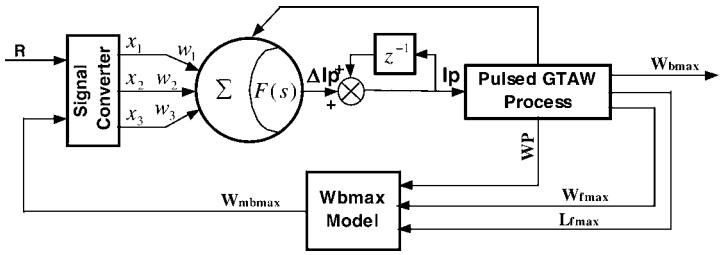

Figure 18. Neuron self-learning PSD control of the backside width of the weld pool.

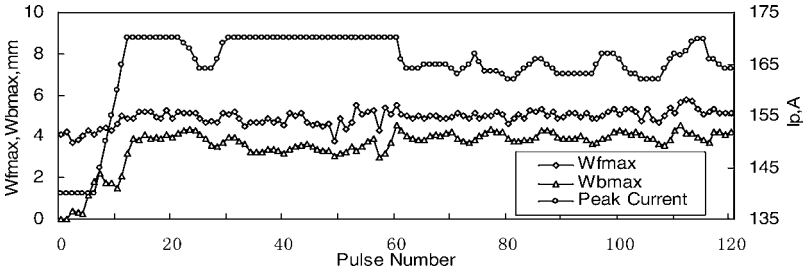

Figure 19. Curve of neuron self-learning PSD control for backside width during robotic pulse GTAW.

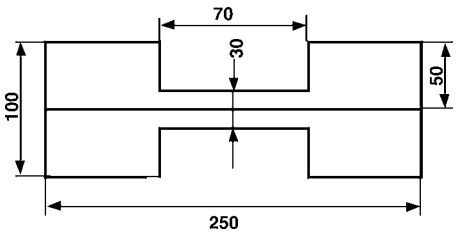

(a)

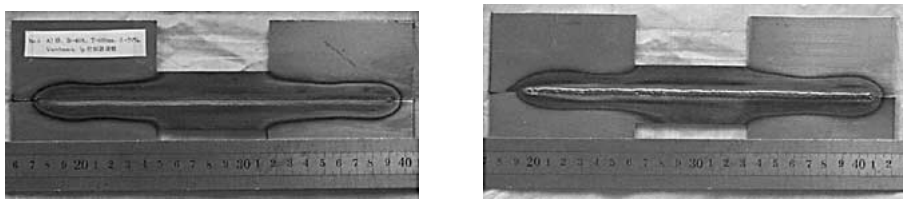

(b) (c)

Figure 20. Photographs of neuron self-learning PSD controlling for backside width of dumb-bell work-piece: (a) shape and the size of the work-piece; (b) topside; (c) backside.

and processing variables. The error and its changes between predicted and measured maximum backside pool width were inputs of the neuron self-learning PSD controller.

The work-piece was dumb-bell-shaped mild steel plate of 2 mm thickness. The size and the shape of the work-piece are shown in Figure 20(a). The peak current value of the pulse was regulated by the neuron self-learning PSD controller during the welding process. The pulse cycle was 0.6 s, and the pulse duty ratio was 50%. The other welding conditions are shown in Table I.

During the controlled welding process, the varying curves of W_{fmax}, W_{mbmax} and control variable, the peak current value, are shown in Figure 19. Maximum backside width supposed was 4.0 mm. Figure 19 shows that the maximum absolute error was 0.81 mm, average error was -0.27 mm and RMS error was 0.47 mm. Photographs of the work-piece are shown in Figures 20(b) and (c).

6. Conclusions

Aimed at the shortcomings of the current teaching play-back welding robot without real-time sensing control of weld pool dynamics, in this study, welding robot systems with real-time visual sensing and self-learning neuron control of weld pool dynamics has been established. The clear pool images of pulsed GTAW during robotic welding were acquired by the visual sensor and composite filter technique. The related image-processing algorithm was developed. Dynamic models of the topside and backside weld pools of pulsed GTAW were established by artificial neural networks. The neuron self-learning PSD controller was designed for ideal topside and backside weld pool characteristics, respectively in real-time. The above results will be key prepared technologies for intelligent welding robots in our further researches.

Acknowledgement

The authors wish to thank the anonymous reviewers for their valuable comments on the earlier draft of this paper.

References

1. Chen, S. B., Lou, Y. J., Wu, L., and Zhao, D. B.: Intelligent methodology for sensing, modeling and control of pulsed GTAW: Part 1 – bead-on-plate welding, *Welding J.* **79**(6) (2000), 151–163.
2. Chen, S. B., Wu, L., and Wang, Q. L.: Self-learning fuzzy neural networks for control of uncertain systems with time delays, *IEEE Trans. Systems Man Cybernet., Part B: Cybernetics* **27**(1) (1997), 142–148.
3. Chen, S. B., Zhao, D. B., Wu, L., and Lou, Y. J.: Intelligent methodology for sensing, modeling and control of pulsed GTAW: Part 2 – butt joint welding, *Welding J.* **79**(6) (2000), 164–174.
4. Kopacek, P.: Intelligent manufacturing: Present state and future trends, *J. Intelligent Robotic Systems* **26**(3) (1999), 217–229.
5. Kovacevic, R. and Zhang, Y. M.: Real-time image processing for monitoring the free weld pool surface, *ASME J. Manufacturing Sci. Engrg.* **119**(5) (1997), 161–169.
6. Kovacevic, R., Zhang, Y. M., and Ruan, S.: Sensing and control of weld pool geometry for automated GTA welding, *ASME J. Engrg. Industry* **117**(2) (1995), 210–222.

7. Lim, T. G. and Cho, H. S.: Estimation of weld pool sizes in GMA welding process using neural networks, in: *The 3rd Internat. Conf. on Trends in Welding Research*, Gatlinburg, TN, 1993, pp. 135–142.
8. Murakami, S.: Weld-line tracking control of arc welding robot using fuzzy logic controller, *Fuzzy Sets Systems* **32**(2) (1989), 31–36.
9. Pietrzak, K. A. and Packer, S. M.: Vision-based weld pool width control, *ASME J. Engrg. Industry* **116** (1994), 86–92.
10. Przakovic, D. and Khani, D. T.: Weld pool edge detection for automated control of weld, *IEEE Trans. Robotics Automat.* **7**(3) (1991), 397–403.
11. Suga, Y., Mukai, M., and Usui, S.: Measurement of molten pool shape and penetration control applying neural network in TIG weld of thin steel plate, *ISIJ Internat.* **39**(10) (1999), 1075–1080.
12. Suga, Y., Mukai, M., Usui, S., and Ogawa, K.: Estimation and adaptive control of penetration in GTAW by monitoring dimension of molten pool, in: *Proc. of the Internat. Conf. on Offshore Mechanics and Arctic Engineering – OMAE*, Vol. 3, 13–17 April 1997, ASME, pp. 95–100.
13. Suga, Y. and Naruse, M.: Application of neural network to visual sensing of weld line and automatic tracking in robot welding, *Welding in the World* **34** (1994), 275–284.
14. Suzuki, A., Hardt, D. E., and Valavani, L.: Application of adaptive control theory to on-line GTA weld geometry regulation, *ASME J. Dyn. Systems Measm. Control* **113**(1) (1991), 93–103.
15. Tzafestas, C. S. and Tzafestas, S. G.: Intelligent robotic assembly and disassembly: General architecture and implementation case studies, in: S. G. Tzafestas (ed.), *Advances in Manufacturing: Decision, Control and Information Technology*, Springer, Berlin/London, 1999, pp. 267–282.
16. Tzafestas, S. G. and Kyriannakis, E.: Regulation of GMA welding thermal characteristics via a hierarchical MIMO predictive control scheme assuring stability, *IEEE Trans. Industr. Electron* **47**(3) (2000), 668–678.
17. Tzafestas, S. G., Raptis, S., and Pantazopoulos, J.: A vision-based path planning algorithm for a robot-mounted welding gun, *Images Process. Commun.* **2**(4) (1996), 61–72.
18. Vilkas, E. P.: Automation of gas tungsten arc welding process, *Welding J.* **45**(5) (1966), 410–416.